Broadly permissive intestinal chromatin underlies lateral inhibition and cell plasticity

Published in final edited form as:
Nature. 2014 February 27; 506(7489): 511–515. doi:10.1038/nature12903.

Broadly permissive intestinal chromatin underlies lateral inhibition and cell plasticity

Tae-Hee Kim[1,2], **Fugen Li**[1], **Isabel Ferreiro-Neira**[1,2], **Li-Lun Ho**[1,2], **Annouck Luyten**[1,2], **Kodandaramireddy Nalapareddy**[1,2], **Henry Long**[1], **Michael Verzi**[1,2], and **Ramesh A. Shivdasani**[1,2,‡]

[1]Department of Medical Oncology and Center for Functional Cancer Epigenetics, Dana-Farber Cancer Institute, Boston, MA 02215, USA

[2]Department of Medicine, Brigham & Women's Hospital and Harvard Medical School, Boston, MA 02215, USA

Abstract

Cells differentiate when transcription factors (TFs) bind accessible *cis*-regulatory elements to establish specific gene expression programs. In differentiating embryonic stem (ES) cells, chromatin at lineage-restricted genes becomes sequentially accessible[1-4], probably by virtue of "pioneer" TF activity[5], but tissues may utilize other strategies *in vivo*. Lateral inhibition is a pervasive process in which one cell forces a different identity on its neighbors[6], and it is unclear how chromatin in equipotent progenitors undergoing lateral inhibition quickly enables distinct, transiently reversible cell fates. Here we report the chromatin and transcriptional underpinnings of differentiation in mouse small intestine crypts, where Notch signaling mediates lateral inhibition to assign progenitor cells into absorptive or secretory lineages[7-9]. Transcript profiles in isolated LGR5$^+$ intestinal stem cells (ISC)[10] and secretory and absorptive progenitors indicated that each cell population was distinct and the progenitors specified. Nevertheless, secretory and absorptive progenitors showed comparable levels of H3K4me2 and H3K27ac histone marks and DNaseI hypersensitivity - signifying accessible, permissive chromatin - at most of the same *cis*-elements. Enhancers acting uniquely in progenitors were well-demarcated in LGR5$^+$ ISC, revealing early priming of chromatin for divergent transcriptional programs, and retained active marks well after lineages were specified. On this chromatin background, ATOH1, a secretory-specific TF, controls lateral inhibition through Delta-like Notch ligand genes and also drives numerous secretory lineage genes. Depletion of ATOH1 from specified secretory cells converted them into functional enterocytes, indicating prolonged responsiveness of marked enhancers to presence or absence of a

‡**Corresponding author:** Ramesh A. Shivdasani, MD, PhD Dana-Farber Cancer Institute 450 Brookline Avenue Boston, MA 02215 (USA) Ph. (617) 632-5746 Fax (617) 582-7198 ramesh_shivdasani@dfci.harvard.edu.

AUTHOR CONTRIBUTIONS

T.H.K. conceived and designed experiments, collected and analyzed data, and drafted the manuscript; F.L. performed computational analyses; I.F.N. performed some mouse experiments; L.L.H, A.L., K.N., and M.V. prepared some ChIP-seq libraries; H.L. supervised computational analyses; R.A.S. conceived and supervised the study, analyzed data, and wrote the manuscript.

Data are deposited in the Gene Expression Omnibus (GSE 51464). The authors declare no conflicts of interest.

key TF. Thus, lateral inhibition and intestinal crypt lineage plasticity involve interaction of a lineage-restricted TF with broadly permissive chromatin established in multipotent stem cells.

Keywords

Tissue differentiation; intestinal crypts; Notch signaling; ATOH1; Lgr5 stem cells

Intestinal crypts produce enterocyte (ENT) and secretory (enteroendocrine, goblet – GOB – or Paneth) lineages after bipotential progenitors start to express ATOH1 and Delta-like ligands, which activate Notch receptors on adjacent cells[8,9]. Notch signaling silences *Atoh1* in recipient cells and within 6 hr ATOH1$^+$ cells adopt the secretory fate, whereas ATOH1$^-$ cells become enterocytes[9,11,12] (Extended Data Fig. 1a); forced ATOH1 expression in mouse fetal intestines promotes secretory differentiation[13]. To investigate the chromatin basis for ATOH1's deterministic activity in lateral inhibition, we purified workhorse LGR5$^+$ ISC from *Lgr5$^{GFP\text{-}Cre}$* mouse crypts[10] (Extended Data Fig. 1b-c). Exploiting a total absence of secretory cells in *Atoh1$^{-/-}$* intestines[11,12,14] (Extended Data Fig. 1d-e), we also harvested mature villus ENT (Fig. 1f) and their crypt progenitors (Ent-Pro, Fig. 1l) from *Villin-Cre^{ER};Atoh$^{Fl/Fl}$* mice (Extended Data Table 1). To expand Sec-Pro, we separately depleted transcription factor RBPJ, which mediates Notch responses[6,7], or disrupted Notch signaling with the γ-secretase inhibitor dibenzazepine (DBZ)[7,15]. Both approaches induced replication arrest and an excess of all secretory cell types[12,16] (Figs. 1e and 1q; Extended Data Figs. 1f and 2). Four days after induced *Rbpj* deletion or 72 h after administration of DBZ, secretory cells appeared in all crypts, but not yet on villi (Fig. 1d, Extended Data Fig. 2), revealing their origins in Sec-Pro. Accordingly, 1 day (*Rbpj$^{-/-}$*) or 1.5 day (DBZ) earlier, crypts uniformly showed high ATOH1 expression, ongoing cell replication, and negligible avidity for the goblet cell (GOB) stain Alcian blue (Figs. 1b-c, 1h-i, 1n-o). Confirming that these ATOH1$^+$ cells are *bona fide* Sec-Pro, they robustly expressed known secretory genes[17] (e.g., *Neurog3*, *Gfi1*, *Spdef*); moreover, Sec-Pro produced in different ways had similar expression profiles, distinct from characteristic transcripts enriched in other cell populations (Extended Data Fig. 3; Supplementary Information Table 1). Although LGR5$^+$ ISC, Sec-Pro, and Ent-Pro share many transcripts, the divergent cell sources and expression profiles indicate that they represent discrete, specified crypt populations.

We used chromatin immunoprecipitation with deep sequencing (ChIP-seq) to first identify sites carrying H3K4me2, a robust mark of functional *cis*-element activity[18,19]. As mammalian genes are controlled mainly through distant enhancers[20], where tissue-restricted TFs bind DNA[21], we concentrated on regions >2 kb upstream or >1 kb downstream of transcription start sites (TSSs). Highly concordant enhancer profiles in independent Ent-Pro replicates and in Sec-Pro obtained after genetic or chemical Notch inhibition (Fig. 2a-b; Extended Data Fig. 4) gave confidence in epigenome analysis of primary cells. As prevailing concepts predict, villus cells clustered farthest in aggregate analysis of H3K4me2-marked enhancers (Fig. 2b) because many enhancers were marked in mature ENT and GOB, but not in their progenitors (Group 2 in Fig. 2a; Extended Data Fig. 5a); these enhancers, delineated only in mature cells, showed significant TF motif enrichment (Supplementary Information Table 2). To our surprise, not only were many enhancers

prominently marked in progenitor cells, but H3K4me2 showed strikingly similar distributions in Sec-Pro and Ent-Pro (Group 1 in Fig. 2a; Extended Data Fig. 5b). Marks were evident at these sites even in LGR5^{+} ISC, distinct from the Group 2 profile, and aggregate analysis verified significant overlap of H3K4me2 enhancers among crypt populations (Fig. 2b). Sites that seemed superficially better marked in DBZ-derived Sec-Pro (Group 1b) lacked TF motif enrichment or other distinguishing features and Sec-Pro-restricted genes were not enriched near these sites but distributed among enhancers marked in all 3 crypt populations (Fig. 2a and Supplementary Information Tables 1 and 2).

As H3K4 is methylated at both poised and active *cis*-elements in ES cells[1], the striking overlap in progenitor cell marks might reflect enhancer *potential*, distinct from enhancer *activity*; H3K27ac is thought to mark active enhancers specifically[22,23]. Though many H3K4me2-marked enhancers lacked H3K27ac, global and local distributions of the latter were remarkably similar in Sec-Pro and Ent-Pro (Fig. 2c-d). DNaseI-hypersensitivity (DHS - an independent, direct measure of chromatin access)[24] was evident at most H3K4me2 sites and its distribution also highly similar in Sec-Pro and Ent-Pro (Fig. 2c-d), distinct from DHS in other mouse tissues (Extended Data Fig. 5c). Thus, thousands of enhancers for lineage-restricted genes show comparable histone activation and tissue-specific chromatin access in distinct, specified crypt progenitors and most such sites carry H3K4me2 in ISC. This early, indiscriminate delineation of enhancers offers a compelling explanation for crypt cell equipotency, a key feature of lateral inhibition, and reveals that intestinal lineage separation does not require differential chromatin priming in daughter cells and may instead rely principally on TF activity.

ATOH1, a Sec-Pro-specific TF, is an ideal candidate to confer selectivity (Extended data Fig. 6a). FLAG ChIP-seq in Sec-Pro isolated from *Atoh1^{Flag}* mice[25] identified thousands of binding sites, most of them in highly conserved, distant enhancers carrying ATOH1 consensus motifs (Extended Data Figs. 4b, 6b) and different from ATOH1 binding sites in cerebellar neurons[25] (Fig. 3a). Intestinal and neuronal binding sites coincided with tissue-specific H3K4 methylation (Extended Data Fig. 6c), attesting to the regulatory significance of this histone modification. Lateral inhibition requires *Atoh1* repression in Notch-recipient cells and ATOH1 activity in Sec-Pro[12,14], and the rapidity of ATOH1-induced lineage divergence[9] hints that it may directly regulate genes driving lateral inhibition. Indeed, ATOH1 bound strongly to its own locus and those for Notch ligands *Dll1* and *Dll4* (Fig. 3b), but not Ent-Pro-specific loci such as *Bcl215* (Extended Data Fig. 6d). These findings support a cell-intrinsic, ATOH1-dependent mechanism for lateral inhibition and a simple, direct means for feed-forward maintenance of this bistable system[26]. ATOH1 also bound numerous loci implicated in secretory differentiation, including determinants of each sub-lineage, and the corresponding transcripts are low or absent in *Atoh1$^{-/-}$* crypts (Fig. 3b; Extended Data Fig. 6e-f). Strong, specific association of ATOH1 binding with Sec-Pro-restricted transcripts further implies that it activates secretory genes without binding or directly repressing ENT genes (Extended Data Fig. 6g).

H3K4me2, H3K27ac, and DHS signals at ATOH1-bound enhancers were, on average, equally strong in ATOH1^{+} Sec-Pro and Ent-Pro, which categorically lack ATOH1 (Fig. 3c). Few secretory loci showed modestly stronger features in Sec-Pro or GOB (Extended Data

Fig. 5d), but most profiles were similar in LGR5^{+} ISC and both progenitors (Fig. 3d). Although in villus cells ATOH1 preferred sites marked only in GOB over those marked only in ENT, in crypts it overwhelmingly favored enhancers bearing H3K4me2 in all populations (Extended Data Fig. 7). The pervasive demarcation of ATOH1-bound enhancers in *Atoh1*$^{-/-}$ Ent-Pro reveals that this TF does not initiate or maintain chromatin access in crypt cells.

The extreme overlap of Sec-Pro and Ent-Pro enhancer profiles indicates persistence of cis-element marks after lineage specification. Intestinal lineages might therefore remain plastic beyond the period of lateral inhibition and sustained chromatin access might explain why some differentiated crypt cells readily assume stem-cell properties[17,27,28]. Our findings particularly suggest that chromatin in specified cells may stay responsive to presence or absence of ATOH1. In *Atoh1*-null fetal intestines, an *Atoh1*^{LacZ} allele is expressed in ENT[14], but this finding could represent a non-cell-autonomous effect of abortive lateral inhibition. We postulated prolonged, cell-autonomous ATOH1 control of lineage identity in specified cells.

To test this hypothesis, we suppressed Notch in *Atoh1*$^{Fl/Fl}$;*Villin-Cre*^{ER} mice and waited past the period of widespread Sec-Pro differentiation before administering tamoxifen to induce *Atoh1* deletion; we also injected bromodeoxyuridine (BrdU) to monitor cell replication and turnover (Fig. 4a). Crypts and villus bases in control *Atoh1*$^{Fl/Fl}$;Cre^{-} mice became filled with non-replicating GOB 3 days after Notch inhibition, as expected (Fig. 4b-d), whereas ATOH1-depleted crypts showed substantial proliferation and many fewer Alcian blue-avid cells (Fig. 4e-g). To demonstrate that this marked difference from control mice did not represent rescue by a few ISC that might have eluded Notch inhibition but rather secretory cell conversion to ENT, we followed cells for 3 additional days (Fig. 4a). By this time Notch-inhibited control *Atoh1*$^{Fl/Fl}$;Cre^{-} mice became moribund and had short villi containing only GOB that showed no BrdU labeling (Fig. 4h-k). Meanwhile, in the absence of Notch suppression, BrdU tracer in wild-type or *Atoh1*$^{-/-}$ intestines had moved from crypts into villus tips (Extended Data Fig. 8a-d), as expected. *Atoh1*$^{Fl/Fl}$;*Villin*$^{Cre-ER}$ mice remained fit and carried only alkaline phosphatase (ALPI)-expressing ENT on tall villi with abundant BrdU signal at the tips (Fig. 4l-o). Thus, ATOH1 loss had overcome secretory fate and replication arrest more than 2 days after Notch inhibition to become Ent-Pro that proliferated and matured into functional ENT.

To verify cell-autonomous fate conversion, we used progesterone/RU486-responsive *Atoh1*$^{Cre-PR}$ mice[29]. Following RU486 injection, YFP signals in control *Atoh1*$^{Cre-PR/+}$;*Rosa26*^{YFP} mice were confined to few GOB and enteroendocrine cells, indicating weak but restricted Cre activity; 4 independent mice never labeled ENT or cell stripes, crucially confirming absence of leaky Cre activity in ISC or multipotent progenitors (Extended Data Fig. 8e-f). We suppressed Notch in *Atoh1*$^{Cre-PR/Fl;}$*Rosa26*^{YFP} mice, then activated Cre selectively in ATOH1^{+} secretory cells, thus deleting the floxed *Atoh1* allele and simultaneously activating a fluorescent lineage tracer (Fig. 4p). Four days later, stripes of YFP^{+} cells emanated from crypts and 95% ± s.d.4.1% of YFP^{+} ATOH1-depleted cells (*N*=1,200 cells; 4 mice) in these ribbons lacked the GOB marker TFF3 but expressed ALPI (Fig 4q-s; Extended Data Fig. 8g), confirming *bona fide* conversion of secretory cells to

ENT. Thus, specified secretory cells are not irrevocably committed and their switched identity upon ATOH1 withdrawal mirrors the broadly permissive chromatin in crypt cells.

Mathematical modeling suggests that bifurcating valleys in Waddington's famous epigenetic landscape best represent reversible nodes, a hallmark of lateral inhibition[26]. The broad priming of ISC and progenitor cell enhancers offers a satisfying explanation for this property in intestinal crypts and accounts for ATOH1 activity in both lateral inhibition and secretory differentiation. ATOH1 reinforces its own expression and directly regulates *Dll1* and *Dll4*, thus enabling Notch-dependent *Atoh1* repression in neighboring cells; its subsequent activity at primed *cis*-elements triggers numerous secretory genes. Sustained enhancer priming allows ATOH1 activity or its absence, which respectively promotes or represses secretory differentiation[13], to affect the fate of specified cells, and DNA methylation also barely changes as ISC differentiate[30]. True lineage commitment thus occurs late, if ever, in the intestinal epithelium. Indeed, various stimuli revert differentiated cells into ISC with surprising ease[17,27,28], implying that the environment, and not some cell-intrinsic feature, determines crypt cell potential. Broadly delineated enhancers likely underlie this remarkable plasticity.

METHODS

Animals and drug administration

Mouse strains were purchased from The Jackson Laboratory or received as gifts and are referenced in Extended Data Table 1. Mice, maintained under specific pathogen–free conditions, were handled in accordance with protocols approved and monitored by the Dana-Farber Cancer Institute Animal Care and Use Committee. Male and female C57BL/6 mice were used between 2 and 6 months of age. Dibenzazepine (DBZ, Syncom, Groningen, The Netherlands) was suspended in 0.5% (w/v) hydroxypropylmethyl-cellulose (Methocel E4M, Dow Chemicals) and 0.1% (w/v) Tween 80 (Bio-Rad) in water and 100 μmol/kg was administered by intraperitoneal (IP) injection. We activated Cre-ER recombinase by IP injection of 1 mg tamoxifen (Invitrogen) for 5 days or one dose of 4 mg tamoxifen. Cre-PR recombinase was induced by 2 IP injections of 2 mg RU486 (Sigma) approximately 8 h apart. BrdU (B-D Biosciences, 50 mg/kg) was injected IP and mice were sacrificed 1 h or 3 days later.

Cell isolation

Epigenomes were characterized in cells isolated from the first half of the small intestine. **LGR5^{+} ISC:** Intestinal villi in *Lgr5$^{GFP\text{-}IRES\text{-}Cre}$* mice[10] were scraped away using glass slides, crypt epithelium was collected by shaking in 5 mM EDTA for 50 min at 4°C, and single-cell suspensions prepared by digestion in 4X TrypLE (Invitrogen) for 50 min at 37°C. GFP^{hi} (LGR5^{+}) cells were sorted using a MoFlo instrument (Beckman Coulter). **Sec-Pro and GOB:** Villi were scraped from intestines of wild-type mice 38 h after intraperitoneal (IP) injection of DBZ (Syncom, 100 μmol/kg i.p.) and crypt cells isolated by shaking residual, crypt-enriched tissue in 5 mM EDTA for 50 min at 4°C. *Rbpj$^{Fl/Fl}$;Villin-Cre^{ER}* mice were injected with 2 daily IP doses of 2 mg tamoxifen, followed by isolation of crypt Sec-Pro as above on the third day, or with 5 daily doses of 1 mg tamoxifen, followed by

isolation of villus GOB on the 10th day. The latter were collected by shaking intestines gently in 5 mM EDTA for 30 min at 4°C, followed by passage through 70 μm filters to eliminate contaminating crypts. **Ent-Pro and ENT:** Crypt epithelial cells and mature ENT were collected from *Atoh1*$^{Fl/Fl}$;*Villin-Cre*^{ER} intestines 14 days after tamoxifen treatment, as described for other mice.

ChIP-seq and DHS-seq

For ChIP-seq, cells were fixed immediately in 1% formaldehyde with rotation for 25 min at ambient temperature and lysed in 1% SDS, 10 mM EDTA, 30 mM Tris-HCl pH8, with protease inhibitors (Roche). Lysates were sonicated using a Bioruptor instrument (Diagenode) for 50 min with 30 s intervals and then incubated overnight at 4°C in dilution buffer (1% Triton, 0.5 M EDTA, 5 M Nacl, 1 M Tris-HCl pH8, protease inhibitors) with Dynabeads (Life Technologies) bound to H3K4me2 (Millipore 07-030), H3K27ac (Abcam ab4729), or FLAG (Sigma F3165) antibodies. Beads were washed and cross-links were reversed in 1% SDS in 0.1 M $NaHCO_3$ for 8 h at 65°C. DNA was purified using quickPCR spin kits (Qiagen) and libraries constructed using ThruPLEX-FD kits (Rubicon Genomics), followed by deep sequencing on a HiSeq2000 instrument (Illumina). For DNaseI-hypersensitive (DHS)-Seq, nuclei were isolated after incubation of epithelial cells on ice for 10 min in 0.2% NP-40 in a buffer containing 15 mM Tris-Cl pH 8.0, 15 mM NaCl, 60 mM KCl, 1 mM EDTA, 0.5 mM EGTA, 0.5 mM spermidine, and 0.15 mM spermine. After washing in the same buffer lacking spermidine and spermine, nuclei were digested with 25 U, 40 U or 50 U of DNase I (Roche) in digestion buffer (60 mM $CaCl_2$, 100 mM NaCl, 10 mM $CaCl_2$, 400 mM Tris-HCl) for 5 min at 37°C. Digestion was stopped by adding stop buffer (50 mM Tris-HCl pH 8, 100 mM NaCl, 0.1% SDS, 100 mM EDTA), followed by incubation for 2 h at 55°C with proteinase K (40 μg/ml). DNA was extracted using phenol-chloroform and treated with 1 U RNase (Roche) for 30 min at 37°C. After gel purification of 50-100 bp DNA fragments, libraries were prepared using the ThruPLEX-FD kit (Rubicon Genomics) and sequenced with Illumina HiSeq2000.

ChIP-Seq and DHS-Seq analyses

Sequence tags were aligned to the *Mus musculus* genome, build mm9 and uniquely mapped, non-redundant reads were retained[34,35]. Genomic profiles of DNaseI hypersensitivity (DHS) and histone marks or ATOH1 binding sites were generated using Model-Based Analysis of ChIP-seq 2 (MACS2), with a q-value (false discovery rate, FDR) threshold of 0.01 and default parameters[36,37]. Peaks were refined by requiring >5-fold enrichment in comparisons with input DNA for ChIP-seq and local backgrounds for DHS-seq. For analyses centered on ChIP peaks, non-promoter (>2 kb upstream or <1 kb downstream from any TSS) peaks from all study samples were merged to create a union set. Read densities (in reads per 1M tags within fixed, 200-bp bins, RPM) were calculated by normalizing counts in each peak region in the union set based on sample sequencing depth. Meta-analyses around ATOH1 binding sites were performed in the Cistrome pipeline[38]. Genomic wiggle traces were normalized for sample sequence depth. Similarities among H3K4me2-marked enhancers in different cell types were determined by hierarchal clustering using Spearman's rank correlation.

Expression analyses and correlation with Atoh1 occupancy

RNA was extracted from LGR5^{+} ISC, Sec-Pro, Ent-Pro, GOB and ENT with Trizol (Invitrogen) and RNeasy Mini Kits (Qiagen), processed, and hybridized to Mouse Genome 430A 2.0 microarrays (Affymetrix). Data quality was verified using Affy QC Report in R bio-conductor. mRNA profiles were analyzed by RMA to normalize expression indices[39], and differential expression across cell types was identified using LIMMA[40] by F test with p <0.002. Values in the expression heatmap (Extended Data Fig. 3) were normalized by magnitude normalization and cell-type specificity was determined by k-means clustering of differentially expressed genes. ATOH1 binding at enhancers was used as a function to determine if ATOH1 activates Sec-Pro-specific genes. Each ATOH1 enhancer (>2 kb upstream or <1 kb downstream from a TSS) was assigned to a nearby gene (TSS <20 kb from an ATOH1 summit). After normalization of tags for sequence depth and peak width, the sum of tag densities for each gene was used to measure its correlation with differential expression.

Histology, immunohistochemistry, and immunofluorescence

Mouse jejuni (middle 1/3 of the small intestine) were fixed overnight in 4% paraformaldehyde at 4°C and embedded in paraffin. Rehydrated 5 μm sections were stained with Alcian blue (Sigma) and nuclear fast red (Sigma). For immunohistochemistry, antigens were retrieved in 10 mM sodium citrate buffer (pH 6). Tissue sections were permeabilized with 0.5% Triton X-100 (Sigma), blocked with 5% fetal calf serum (Gibco), incubated with Ki67 (Vector Laboratories clone MM1, 1:1000), BrdU (AbD Serotec, 1:300), or ATOH1 (gift from Dr. J. Johnson, 1:500) antibodies, and washed in phosphate-buffered saline. Sections were incubated with biotin-conjugated anti-mouse, rat or rabbit IgG (Vector Laboratories, 1:300) and colors developed with Vectastain avidin-biotin complex (Vector) and diaminobenzidine substrate (Sigma). ATOH1 immunostaining was enhanced with the Tyramide Signal Application kit (Perkin-Elmer). For immunofluorescence, tissues embedded in Optimal Cutting Temperature compound (Sakura) were sectioned and incubated with Chromogranin A (ImmunoStar, 1:200), Mucin2 (Santa Cruz, 1:200), or TFF3 (gift from Dr. D. Podolsky, 1:500) antibodies. After washings, samples were incubated with Alexa Fluor 594-conjugated anti-rabbit IgG (Invitrogen). In the lineage conversion experiments in *Atoh1*$^{Cre\text{-}PR/Fl}$;*Rosa26*^{YFP} mice (Fig. 4p-s), tissue sections were stained sequentially with Tff3 Ab and AP substrate.

Extended Data

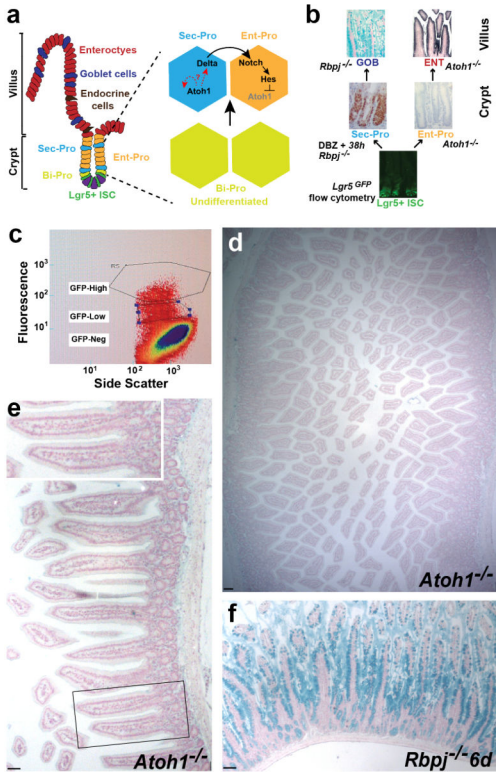

Extended Data Figure 1. Isolation of ISC and other intestinal cells

(a) Crypt-villus unit structure and components of crypt lateral inhibition. Terminally differentiated enterocytes and secretory cells line intestinal villi and depend on self-renewing crypt populations of LGR5^{+} ISC, bipotential (Bi-Pro), and specified secretory (Sec-Pro) and enterocyte (Ent-Pro) progenitors. Stochastic ATOH1 expression in one Bi-Pro induces secretory differentiation and Delta ligand expression, allowing Notch signal delivery to neighboring cells, which use HES1 to repress *Atoh1* and become enterocytes. **(b)** Intestinal epithelial cell isolation strategies. LGR5^{+} ISC were isolated from *Lgr5*$^{GFP\text{-}CreER}$ mice[10]; Sec-Pro and GOB were isolated from *Rbpj*$^{-/-}$ intestines[7]; additional Sec-Pro were collected from DBZ-treated wild-type mouse crypts; Ent-Pro and ENT were harvested from *Atoh1*$^{-/-}$ intestines[14]. **(c)** Crypt cells expressing high LGR5/GFP were isolated by flow cytometry and pooled from 12 mice. Gates to distinguish GFP^{hi} ISC from their GFP^{lo} and GFP^{-} progeny are shown in the representative scatter plot. **(d, e)** Alcian blue staining of *Atoh1*$^{-/-}$ intestines at low (d) and high (e) magnification, demonstrating global absence of GOB. Inset in **e** shows the boxed region at higher magnification. **(f)** *Rbpj*$^{Fl/Fl}$;*Villin-Cre*^{ER} intestines rendered null for Notch activity 6 days after tamoxifen injection, showing severe goblet cell metaplasia, comparable to DBZ-treated wild-type intestines (See Extended Data Fig. 2d). Scale bars, 50 μm. Duplicate samples were examined from 3 (*Rbpj*$^{-/-}$) or 7 (*Atoh1*$^{-/-}$) mice.

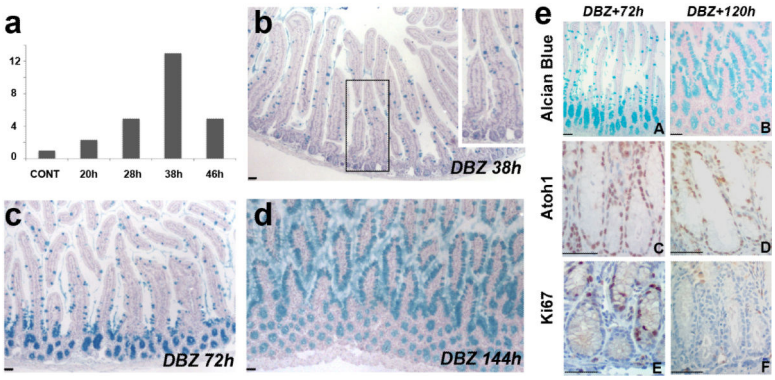

Extended Data Figure 2. Enrichment of Sec-Pro by chemical inhibition of Notch signaling

(a) Quantitative RT-PCR data showing peak *Atoh1* expression ~38 h after treatment of wild-type mice with dibenzazepine (DBZ). **(b-d)** Low magnification views show no increase in mature, Alcian blue-avid goblet cells 38 h after DBZ treatment (b), appearance of goblet cells in villus bases and crypts 72 h after DBZ treatment (c), and migration of these cells to occupy villi almost fully within 6 days (d). Inset in **b** shows a magnified view of the boxed area. **(e)** Within 72 h of DBZ treatment, crypt cells virtually cease to replicate (e-E), retain ATOH1 (e-C), and stain with Alcian blue (e-A), a sign of GOB maturation. By 120 h after DBZ exposure, these ATOH1^{+} post-mitotic GOB occupy short villi (e-B,D,F). Scale bars, 50 μm. Tissue analyses were done in duplicate on 7 (DBZ+38h) or 3 (DBZ+72h, (DBZ +144h) mice.

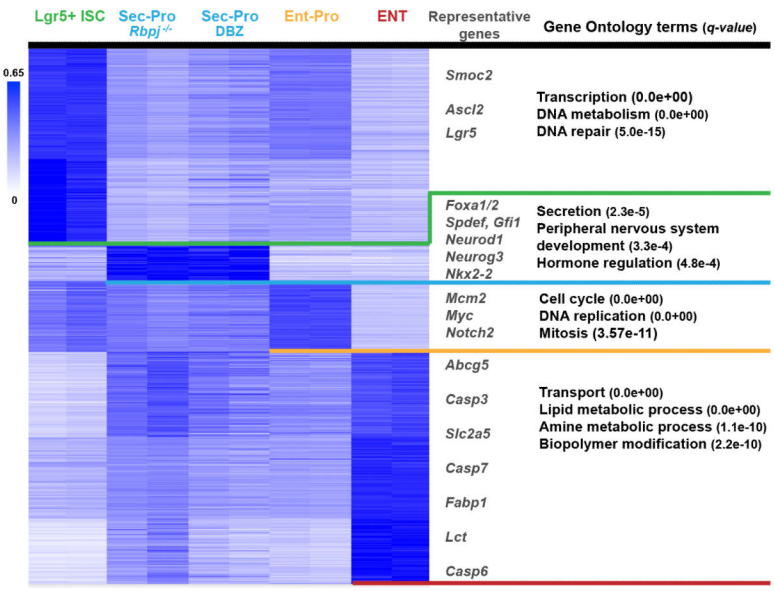

Extended Data Figure 3. Distinct expression profiles in LGR5^{+} ISC, Sec-Pro, Ent-Pro, and villus enterocytes

Differential transcripts in purified intestinal cell types, arranged by K-means clustering of normalized expression values from Affymetrix microarrays. Representative known genes in each cell type are listed alongside the Gene Ontology functions most enriched in each group

(false discovery rates in parentheses), determined using Gene Set Enrichment Analysis tools (http://www.broadinstitute.org/gsea/msigdb/annotate.jsp).

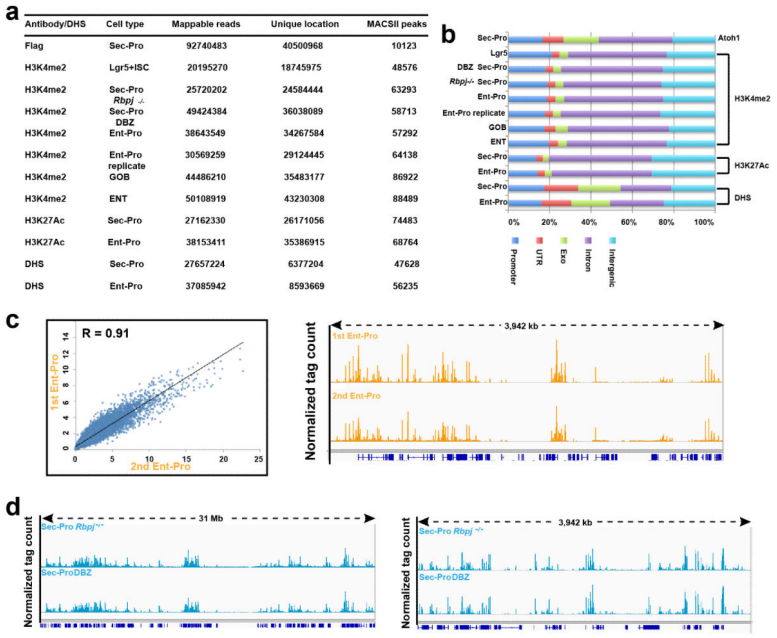

Extended Data Figure 4. Summary of ChIP-seq and DHS-seq experiments

(a) Summary of sites identified by MACS II in ChIP-Seq and DHS-Seq data from intestinal cell populations. **(b)** Distribution of sites marked in promoters (<2 kb upstream or <1 kb downstream of any TSS), coding regions, introns, and intergenic regions. **(c)** Correlation analysis with Spearman's rank coefficient (left) and sample traces (right) of H3K4me2-marked enhancers in independent ChIP-Seq replicates of Ent-Pro, showing very high concordance. **(d)** H3K4me2 ChIP-seq profiles at arbitrarily selected regions of mouse chromosome 17 illustrate the highly concordant signals in Sec-Pro produced by *Rbpj* loss (top traces) or DBZ treatment (bottom traces), as heatmaps and clustering analysis (Fig. 2a-b) demonstrate throughout the genome.

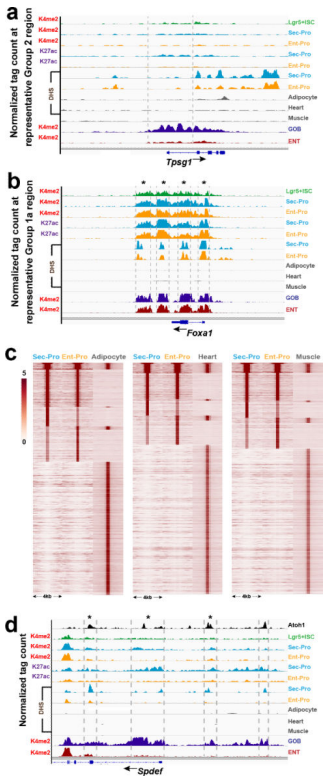

Extended Data Figure 5. Accessible, marked enhancers in intestinal crypt progenitors

(a-b) ChIP-seq and DHS-seq traces at sample secretory loci illustrate selective intron marking in GOB at *Tpsg1* (a), representing the profiles in Group 2 enhancers (Fig. 2a), and highly similar distribution of H3K4me2, H3K27ac, and DHS signals (within dotted, asterisked lines) across cell populations at *Foxa1* (b), representing the prevalent Group 1 pattern. **(c)** Heatmaps of DHS at 116,324 to 139,312 enhancers showing accessible chromatin in Sec-Pro and Ent-Pro, compared to DNAseI insensitivity at the same sites in adipocytes, cardiac, and skeletal muscle (data from the ENCODE Project Consortium, *PLoS Biol* **9**, e1001046 (2011)), and lack of chromatin access in crypt progenitors at enhancers that are active in these heterologous cells. **(d)** At a few secretory loci, such as *Spdef*, signs of enhancer activity and access are higher in *Rbpj*$^{-/-}$ Sec-Pro or GOB than in other intestinal cells. Asterisked intervals mark ATOH1 binding regions.

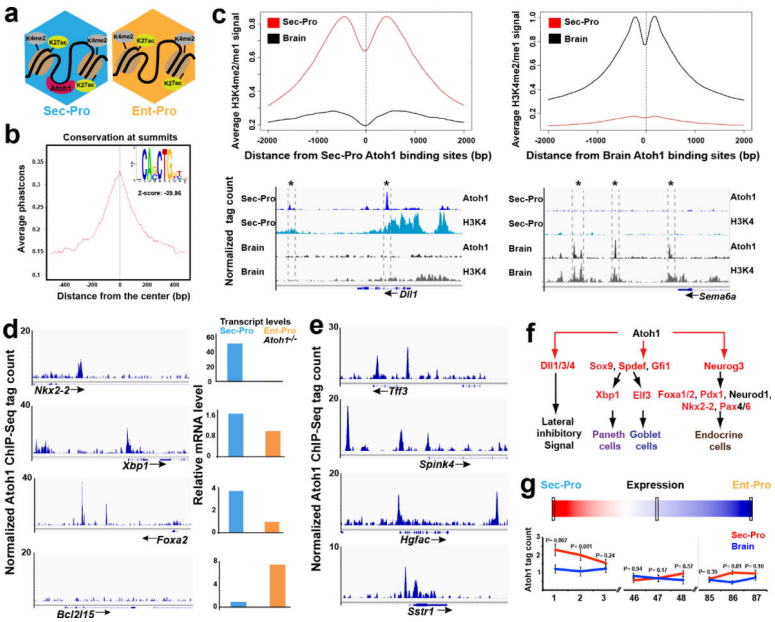

Extended Data Figure 6. ATOH1 transcriptional control of secretory differentiation

(a) Model for cell-specific ATOH1 binding to permissive chromatin in crypt progenitors. **(b)** Phastcons plot showing high evolutionary conservation of ATOH1-occupied sites in Sec-Pro and maximal enrichment of the consensus ATOH1 recognition motif near their peaks. **(c)** Composite profiles of average H3K4me density near ATOH1 binding sites in Sec-Pro (left) and mouse brain (right). H3K4me marks are highly correlated with ATOH1 occupancy in the same, but not in the heterologous, tissue, as representative ChIP-seq data illustrate below. **(d-e)** Examples of ATOH1 occupancy at loci for key secretory lineage TFs and secretory-specific genes: *Nkx2-2* and *Foxa2* (enteroendocrine cells), *Xbp1* (Paneth cells), *Tff3* (goblet cells), *Spink4* and *Hgfac* (goblet and Paneth cells) and *Sstr1* (endocrine cells). ATOH1 does not bind near Ent-Pro-specific genes, as shown at a sample locus, *Bcl2l15*. **(f)** Schematic representation of ATOH1's dual function in direct control of two gene groups: Delta ligands for lateral inhibition and key secretory-specific TFs to promote secretory lineage differentiation. **(g)** Relation of ATOH1 occupancy at enhancers with Sec-Pro-specific transcription. Bins of 200 genes, ranked by differential expression in Sec-Pro (left) or Ent-Pro (right), are represented along the x-axis and normalized ATOH1 binding in Sec-Pro (red) or brain (blue) at enhancers within 20 kb of the genes in each bin is represented on the y-axis. The graphs show the first (Sec-Pro-specific), middle (no differential expression), and last (Ent-Pro-specific) 3 bins of 200 genes each. Pair-wise T tests support a role for ATOH1 in activating Sec-Pro genes, without an overt role in silencing Ent-Pro genes.

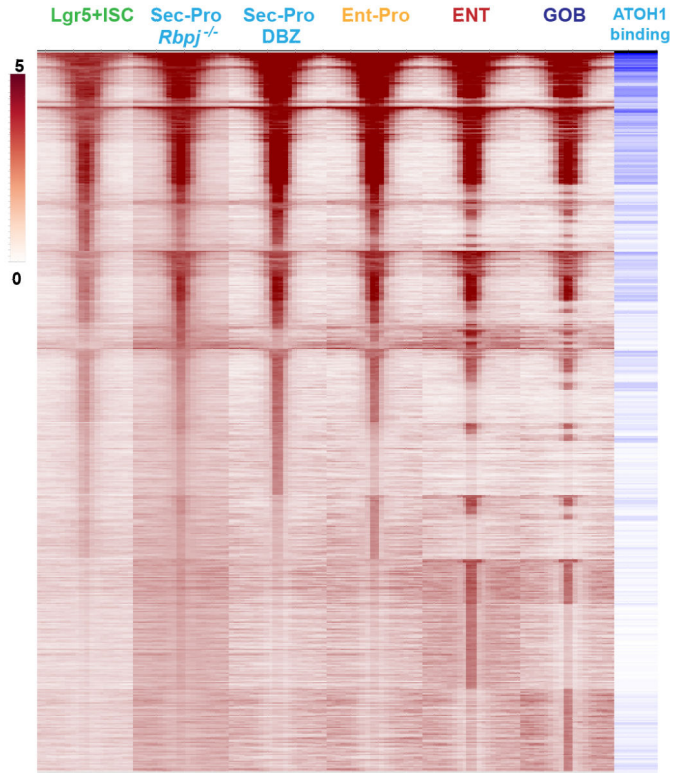

Extended Data Figure 7. ATOH1 binding at H3K4me2-marked enhancers

Representation of ATOH1 binding sites in relation to the heatmap of H3K4me2 marking at 57,481 non-promoter sites (from Fig. 2a), showing that ATOH1 occupies an abundance of sites marked in all crypt populations. Only in mature villus cells does ATOH1 preferentially bind enhancers that are selectively marked in GOB.

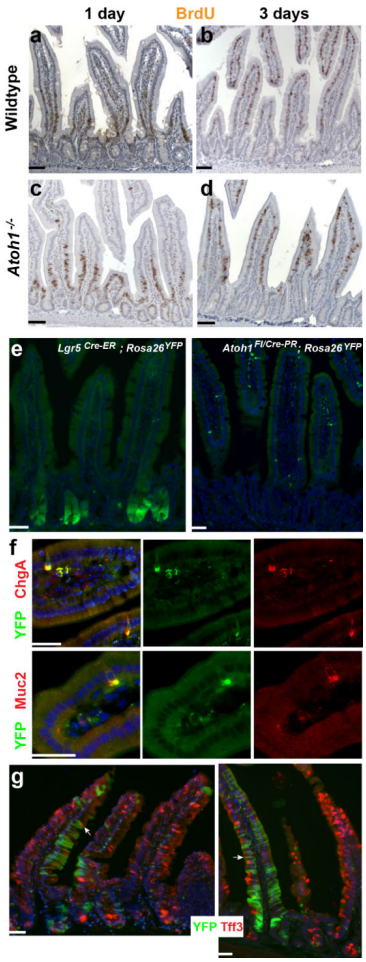

Extended Data Figure 8. ATOH1-dependent lineage conversion

(a-d) BrdU tracing 1 and 3 days after label injection, showing similar turnover of intestinal epithelial cells in wild-type and *Atoh1*-null intestines in the absence of Notch inhibition. Nearly all the label is in the villus base at 1 day and in the top halves of villi at 3 days. **(e)** Lineage tracing 3 days after induction of Cre activity by tamoxifen in $Lgr5^{Cre\text{-}ER}$;$Rosa26^{YFP}$ mice (left) or by RU486 in $Atoh1^{Cre\text{-}PR}$;$Rosa26^{YFP}$ mice (right). YFP is detected in numerous whole crypts (except Paneth cells) in the former, and never in crypts, ribbons or cell pairs in the latter, confirming absence of leaky Cre^{PR} expression in multipotent progenitors. **(f)** YFP signal in $Atoh1^{Cre\text{-}PR}$;$Rosa26^{YFP}$ mice 3 days after RU486-induced Cre activation is confined to scattered $ChgA^{+}$ enteroendocrine and $Muc2^{+}$ GOB cells. **(g)** Two additional representative examples of YFP-traced cell groups that had converted into Tff3-negative ENT after *Atoh1* deletion in secretory cells. Arrows indicate rare (~5%, see text) YFP^{+} cells that still express Tff3. Scale bars, 50 μm. Tissues were analyzed in duplicate from 4 (*Wt*, $Atoh1^{-/-}$, $Atoh^{Cre\text{-}PR/+}$;$Rosa26^{YFP}$) or 6 ($Lgr5^{Cre\text{-}ER}$;$Rosa26^{YFP}$) mice.

Extended Data Table 1

Mouse strains used in this study.

Mouse strain	Features	Application in our study	Ref.
Lgr5$^{GFP\text{-}IRES\text{-}Cre(ER\text{-}T2)}$	Knock-in of a GFP-Cre fusion transcript into the *Lgr5* locus, creating a null, GFP-expressing *Lgr5* allele while retaining one wild-type allele	To isolate GFP^{+} (LGR5^{+}) ISC by flow cytometry	10
Atoh1^{FLAG}	FLAG epitope-tagged *Atoh1* allele created by gene knock-in	ATOH1 ChIP-seq using FLAG antibody	25
Atoh1$^{Cre\text{-}PR}$	Progesterone-inducible Cre recombinase knocked in to the *Atoh1* locus, creating one null Cre-expressing and retaining one wild-type allele	Specific, RU486-inducible Cre activation in ATOH1-expressing crypt epithelial cells, to monitor their fate following *Atoh1* deletion (Fig. 4)	29
Atoh^{Fl}	Conditional (floxed) *Atoh1* allele that is rendered null by Cre-mediated recombination	Intestinal depletion of ATOH1 to eliminate all secretory cells, and hence isolate Ent-Pro from crypts and pure mature enterocytes from villi	14
Rbpj^{Fl}	Conditional (floxed) *Rbpj* allele that is rendered null by Cre-mediated recombination	Alternative, genetic strategy to DBZ-induced Notch inhibition. Induction of total secretory metaplasia to allow isolation of Sec-Pro from crypts and pure mature goblet cells from villi	31
Villin-Cre(ER)	Transgenic mice expressing Cre recombinase selectively in all intestinal epithelial cells, driven by endogenous *Villin* promoter and enhancer elements	To express tamoxifen-responsive Cre recombinase throughout the intestinal epithelium in adult mice	32
Rosa26$^{Lox\text{-}STOP\text{-}LoxYFP}$	Knock-in of Cre recombinase-dependent eYFP cDNA in the ubiquitously expressed, non-essential *Rosa26* locus	To trace ATOH1-expressing crypt cells to follow their choice of secretory *vs.* enterocyte fate (Fig. 4)	33

Supplementary Material

Refer to Web version on PubMed Central for supplementary material.

Acknowledgments

Supported by NIH grants R01DK082889 and R01DK081113 (R.A.S.), K99DK095983 (T.H.K.), K01DK088868 (M.V.), and P50CA127003; a North American Neuroendocrine Tumor Society fellowship (T.H.K.); and the Caring For Carcinoid Foundation (R.A.S.). We thank S. Robine for Villin-Cre$^{ER\text{-}T2}$ mice; T. Honjo and S. Artavanis-Tsakonas for *Rbpj*^{Fl} mice; J. Johnson for ATOH1 antibody; D. Podolsky for TFF3 antibody; and M. Brown and P. Cejas for discussions.

REFERENCES

1. Bernstein BE, et al. A bivalent chromatin structure marks key developmental genes in embryonic stem cells. Cell. 2006; 125:315–26. [PubMed: 16630819]
2. Wamstad JA, et al. Dynamic and coordinated epigenetic regulation of developmental transitions in the cardiac lineage. Cell. 2012; 151:206–20. [PubMed: 22981692]
3. Rada-Iglesias A, et al. Epigenomic annotation of enhancers predicts transcriptional regulators of human neural crest. Cell Stem Cell. 2012; 11:633–48. [PubMed: 22981823]
4. Xie W, et al. Epigenomic analysis of multilineage differentiation of human embryonic stem cells. Cell. 2013; 153:1134–48. [PubMed: 23664764]
5. Zaret KS, Carroll JS. Pioneer transcription factors: establishing competence for gene expression. Genes Dev. 2011; 25:2227–41. [PubMed: 22056668]

6. Artavanis-Tsakonas S, Rand MD, Lake RJ. Notch signaling: cell fate control and signal integration in development. Science. 1999; 284:770–6. [PubMed: 10221902]
7. van Es JH, et al. Notch/gamma-secretase inhibition turns proliferative cells in intestinal crypts and adenomas into goblet cells. Nature. 2005; 435:959–63. [PubMed: 15959515]
8. Pellegrinet L, et al. Dll1- and dll4-mediated notch signaling are required for homeostasis of intestinal stem cells. Gastroenterology. 2011; 140:1230–1240. e1–7. [PubMed: 21238454]
9. Stamataki D, et al. Delta1 expression, cell cycle exit, and commitment to a specific secretory fate coincide within a few hours in the mouse intestinal stem cell system. PLoS One. 2011; 6:e24484. [PubMed: 21915337]
10. Barker N, et al. Identification of stem cells in small intestine and colon by marker gene Lgr5. Nature. 2007; 449:1003–7. [PubMed: 17934449]
11. Yang Q, Bermingham NA, Finegold MJ, Zoghbi HY. Requirement of Math1 for secretory cell lineage commitment in the mouse intestine. Science. 2001; 294:2155–8. [PubMed: 11739954]
12. Kim TH, Shivdasani RA. Genetic evidence that intestinal Notch functions vary regionally and operate through a common mechanism of Math1 repression. J Biol Chem. 2011; 286:11427–33. [PubMed: 21282114]
13. VanDussen KL, Samuelson LC. Mouse atonal homolog 1 directs intestinal progenitors to secretory cell rather than absorptive cell fate. Dev Biol. 2010; 346:215–23. [PubMed: 20691176]
14. Shroyer NF, et al. Intestine-specific ablation of mouse atonal homolog 1 (Math1) reveals a role in cellular homeostasis. Gastroenterology. 2007; 132:2478–88. [PubMed: 17570220]
15. Milano J, et al. Modulation of notch processing by gamma-secretase inhibitors causes intestinal goblet cell metaplasia and induction of genes known to specify gut secretory lineage differentiation. Toxicol Sci. 2004; 82:341–58. [PubMed: 15319485]
16. Kazanjian A, Noah T, Brown D, Burkart J, Shroyer NF. Atonal homolog 1 is required for growth and differentiation effects of notch/gamma-secretase inhibitors on normal and cancerous intestinal epithelial cells. Gastroenterology. 2010; 139:918–28. 928, e1–6. [PubMed: 20621629]
17. van Es JH, et al. Dll1+ secretory progenitor cells revert to stem cells upon crypt damage. Nat Cell Biol. 2012; 14:1099–104. [PubMed: 23000963]
18. Barski A, et al. High-resolution profiling of histone methylations in the human genome. Cell. 2007; 129:823–37. [PubMed: 17512414]
19. Verzi MP, et al. Differentiation-specific histone modifications reveal dynamic chromatin interactions and partners for the intestinal transcription factor CDX2. Dev Cell. 2010; 19:713–26. [PubMed: 21074721]
20. Heintzman ND, et al. Distinct and predictive chromatin signatures of transcriptional promoters and enhancers in the human genome. Nat Genet. 2007; 39:311–8. [PubMed: 17277777]
21. Gerstein MB, et al. Architecture of the human regulatory network derived from ENCODE data. Nature. 2012; 489:91–100. [PubMed: 22955619]
22. Rada-Iglesias A, et al. A unique chromatin signature uncovers early developmental enhancers in humans. Nature. 2011; 470:279–83. [PubMed: 21160473]
23. Creyghton MP, et al. Histone H3K27ac separates active from poised enhancers and predicts developmental state. Proc Natl Acad Sci U S A. 2010; 107:21931–6. [PubMed: 21106759]
24. Boyle AP, et al. High-resolution mapping and characterization of open chromatin across the genome. Cell. 2008; 132:311–22. [PubMed: 18243105]
25. Klisch TJ, et al. In vivo Atoh1 targetome reveals how a proneural transcription factor regulates cerebellar development. Proc Natl Acad Sci U S A. 2011; 108:3288–93. [PubMed: 21300888]
26. Ferrell JE Jr. Bistability, bifurcations, and Waddington's epigenetic landscape. Curr Biol. 2012; 22:R458–66. [PubMed: 22677291]
27. Schwitalla S, et al. Intestinal tumorigenesis initiated by dedifferentiation and acquisition of stem-cell-like properties. Cell. 2013; 152:25–38. [PubMed: 23273993]
28. Buczacki SJ, et al. Intestinal label-retaining cells are secretory precursors expressing Lgr5. Nature. 2013; 495:65–9. [PubMed: 23446353]

29. Rose MF, Ahmad KA, Thaller C, Zoghbi HY. Excitatory neurons of the proprioceptive, interoceptive, and arousal hindbrain networks share a developmental requirement for Math1. Proc Natl Acad Sci U S A. 2009; 106:22462–7. [PubMed: 20080794]
30. Kaaij LT, et al. DNA methylation dynamics during intestinal stem cell differentiation reveals enhancers driving gene expression in the villus. Genome Biol. 2013; 14:R50. [PubMed: 23714178]
31. Han H, et al. Inducible gene knockout of transcription factor recombination signal binding protein-J reveals its essential role in T versus B lineage decision. Int Immunol. 2002; 14:637–45. [PubMed: 12039915]
32. el Marjou F, et al. Tissue-specific and inducible Cre-mediated recombination in the gut epithelium. Genesis. 2004; 39:186–93. [PubMed: 15282745]
33. Srinivas S, et al. Cre reporter strains produced by targeted insertion of EYFP and ECFP into the ROSA26 locus. BMC Dev Biol. 2001; 1:4. [PubMed: 11299042]
34. Langmead B, Trapnell C, Pop M, Salzberg SL. Ultrafast and memory-efficient alignment of short DNA sequences to the human genome. Genome Biol. 2009; 10:R25. [PubMed: 19261174]
35. Zang C, et al. A clustering approach for identification of enriched domains from histone modification ChIP-Seq data. Bioinformatics. 2009; 25:1952–8. [PubMed: 19505939]
36. Zhang Y, et al. Model-based analysis of ChIP-Seq (MACS). Genome Biol. 2008; 9:R137. [PubMed: 18798982]
37. Feng J, Liu T, Qin B, Zhang Y, Liu XS. Identifying ChIP-seq enrichment using MACS. Nat Protoc. 2012; 7:1728–40. [PubMed: 22936215]
38. Liu T, et al. Cistrome: an integrative platform for transcriptional regulation studies. Genome Biol. 2011; 12:R83. [PubMed: 21859476]
39. Irizarry RA, et al. Exploration, normalization, and summaries of high density oligonucleotide array probe level data. Biostatistics. 2003; 4:249–64. [PubMed: 12925520]
40. Smyth GK. Linear models and empirical bayes methods for assessing differential expression in microarray experiments. Stat Appl Genet Mol Biol. 2004; 3 Article3.

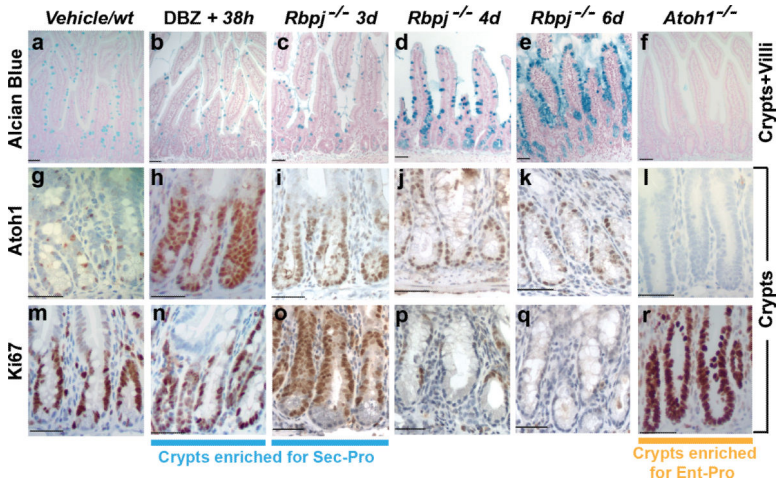

Figure 1. Enrichment of Sec-Pro and Ent-Pro

Approximately 38 h (DBZ treatment) or 3 days (*Rbpj* loss) after Notch inhibition, crypt cells remain proliferative (n,o) but express ATOH1 (h,i) and fail to stain with Alcian blue (b,c), indicating immaturity. By 4 days after *Rbpj* deletion, crypt cells cease replication (p), retain ATOH1 (j), and show weak Alcian blue staining (d); 2 days later, their GOB progeny occupy short villi (e,k,q). *Atoh1*$^{-/-}$ intestines lack secretory cells, carrying only ENT on villi (f) and replicating ATOH1^{-} Ent-Pro in crypts (l,r). Scale bars, 50 μm. Duplicate samples were examined from 3 (*Rbpj*$^{-/-}$ and *WT*) or 7 (DBZ+38h and *Atoh1*$^{-/-}$) mice.

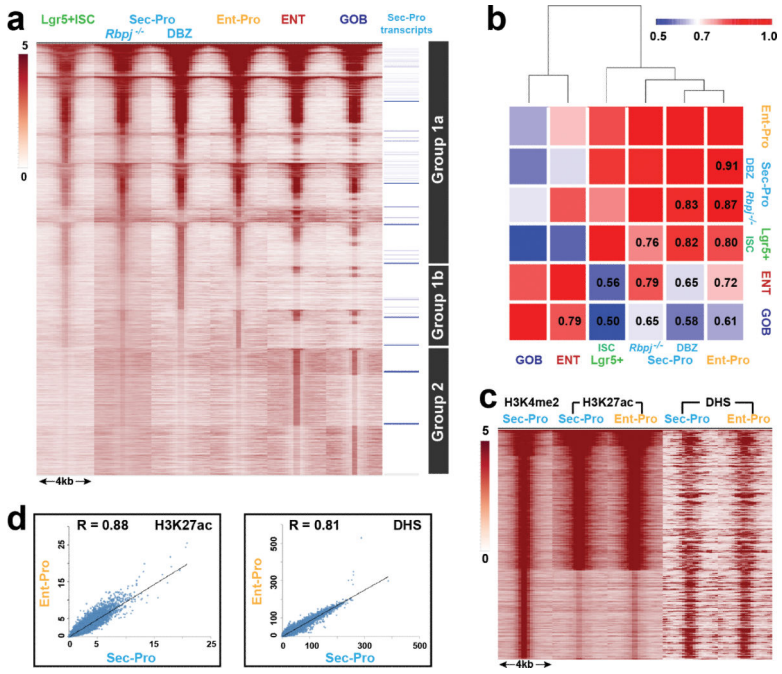

Figure 2. Broadly permissive chromatin in intestinal crypt progenitors

(a) H3K4me2 levels at 57,481 sites (>2 kb upstream or >1 kb downstream of any TSS) are similar in Sec-Pro, Ent-Pro, and LGR5^{+} ISC; Sec-Pro-selective genes are usually marked as strongly in other cells as in Sec-Pro. Groups 1a and 2 denote strongly marked and unmarked enhancers, respectively, in Sec-Pro. Group 1b denotes enhancers with superficially stronger marking in one or other progenitor. **(b)** Hierarchal clustering and Spearman's correlation coefficients for normalized H3K4me2 signals in crypt and villus enhancers. Crypt and villus cells show expected differences, but crypt progenitors and ISC are highly similar. **(c)** H3K27ac and DHS levels at 21,354 enhancers with robust H3K4me2 in *Rbpj*$^{-/-}$ Sec-Pro. Many sites show high H3K27ac and DHS, both similar in Sec-Pro and Ent-Pro. **(d)** High concordance, shown with Spearman's correlation coefficients, between all sites with H3K27ac (33,257 sites) or DHS (116,325 sites) in Sec-Pro and Ent-Pro.

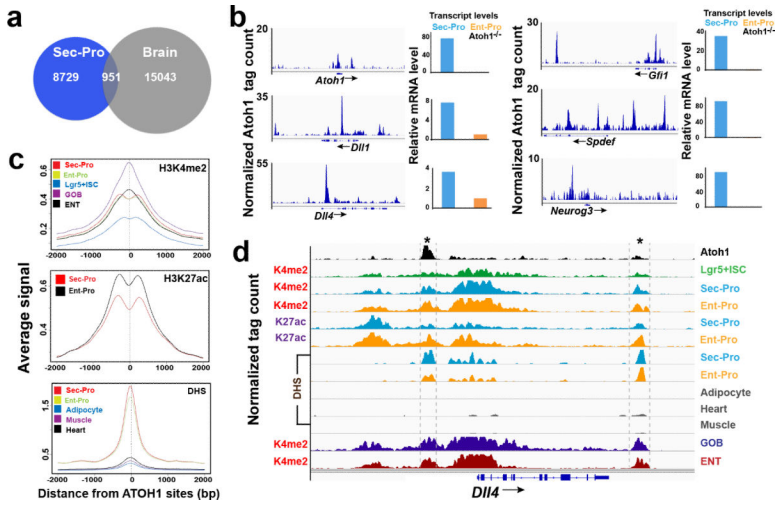

Figure 3. ATOH1 binding and chromatin interactions

(a) Low overlap of ATOH1 binding sites in mouse Sec-Pro and brain. **(b)** ChIP-seq data showing multiple strong ATOH1 binding sites at Sec-Pro-selective *Atoh1*, *Dll1* and *Dll4* genes (left) and at crucial TF genes expressed specifically in Sec-Pro (right). **(c)** Average H3K4me2, H3K27ac, and DHS signals at ATOH1-bound enhancers are comparable in intestinal crypt cell populations, including *Atoh1*-null Ent-Pro. Intestinal DHS sites differ from those in other tissues. **(d)** Data at a representative secretory locus show similar H3K4me2, H3K27ac, and DHS levels in all crypt populations, including at ATOH1-bound enhancers (asterisks and dotted lines).

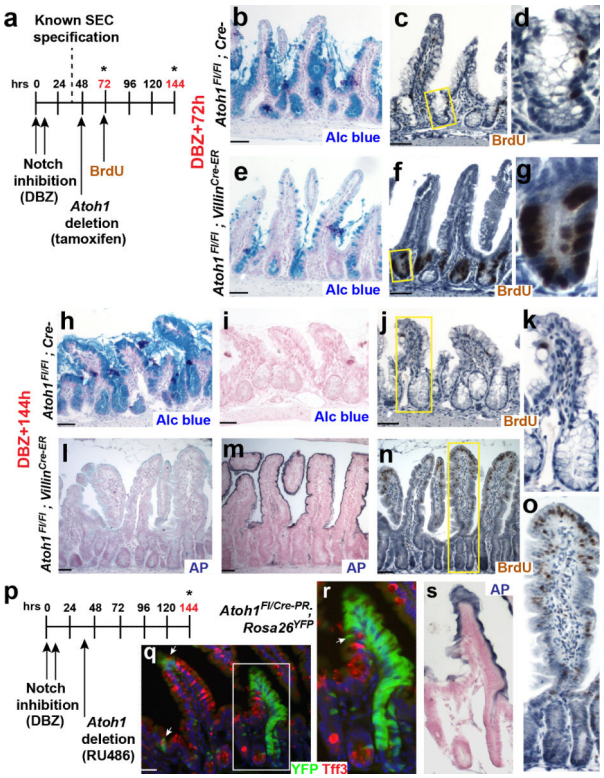

Figure 4. Conversion of specified secretory cells to enterocytes

(a) Notch inhibition (DBZ, 2 doses 6 h apart) and ATOH1 depletion schema in *Atoh1*$^{Fl/Fl}$;*Villin-Cre*^{ER} mice, with BrdU tracing. **(b-g)** Three days after Notch inhibition (1 h post-BrdU), most ATOH1-depleted crypt cells showed BrdU and little Alcian blue staining; Cre^{-} crypt cells had largely stopped replicating and started to mature into GOB. **(h, i, l, m)** Six days after Notch inhibition (3 days post-BrdU), ATOH1-depleted cells had converted globally to enterocytes, showing alkaline phosphatase (AP) but not Alcian blue staining; ATOH1^{+} control intestines showed profound goblet cell metaplasia. **(j, k, n, o)** BrdU, absent in *Atoh1*$^{Fl/Fl}$;*Cre*$^{-}$ intestines, appeared at villus tips in *Atoh1*$^{Fl/Fl}$;*Villin-Cre*^{ER} intestines. Boxes (c, f, j, n) are magnified in adjacent panels. **(p)** Notch inhibition and Sec-Pro-selective *Atoh1* deletion strategy in *Atoh1*$^{Cre\text{-}PR/Fl}$;*Rosa26*^{YFP} mice. **(q-s)** Ribbons of crypt cells originally specified as secretory (YFP^{+}) and then rendered *Atoh1*-null expressed AP but not GOB marker Tff3. The box in **q** is magnified in **r** and **s**; arrows point to rare YFP^{+} Tff3^{+} cells. Scale bars, 50 μm. Duplicate samples were examined from 3 (Cre^{-}: DBZ +72h, DBZ+144h), 9 (*Villin-Cre*, DBZ+72h), 6 (*Villin-Cre*, DBZ+144h), or 4 (*Atoh*$^{Fl/Cre\text{-}PR}$) mice.